

# An Explicit Projection Method for Solving Incompressible Navier-Stokes Equations

S. Detrembleur<sup>1</sup>, B.J. Dewals<sup>1,2</sup>, P. Archambeau, S. Erpicum<sup>1</sup>, M. Pirotton<sup>1</sup>

<sup>1</sup> HACH unit, Department ArGenCo, University of Liege, Belgium, e-mail: sylvain.detrembleur@ulg.ac.be

<sup>2</sup> Belgian Fund for Scientific Research F.R.S.-FNRS

**ABSTRACT:** During the dimensioning of many hydraulic structures, it is from great interest to be able to model in detail the flow near the additional structures such as spillway, hydrants or bottom outlets. The developed software allows the resolution of the incompressible Navier-Stokes equations in the vertical plane of the flow. This program is integrated in the modeling system WOLF, which is fully developed within the unit of the HACH.

This modeling system allows the study of the hydrological process, from the propagation of the rain on the catchment (WOLFHYDRO), the propagation in one-dimensional network (WOLF1D) to the modeling of flow in quasi three-dimensional (WOLF2D) and finally including the developed module (WOLF2DV) described in this paper. This last one offers an additional tool for more localized studies when the resulting fields of pressure deviate from the hydrostatic assumption.

The resolution of the Navier-Stokes equations is carried out on basis of the well-known finite volumes method applied to a regular grid composed of squared meshes. Among the multiple methods of resolution available in the literature, such as implicit methods or pseudo-compressibility ones, the method of projections was adopted.

The numerical implementation of the resolution for the equations is carried out according to an original splitting of the unknowns using a space precision of first or second order. Temporal integration is ensured by Runge-Kutta schemes going up to four steps.

The resolution of the Poisson's equation is ensured by the powerful iterative method of GMRES that makes the solving of big linear systems possible. The implementation described in this paper reached the performance to solve problems containing up to 250,000 computed cells or 750,000 unknowns in a very short computing time.

Moreover, the viscous diffusive terms are integrated into the model, allowing the explicit computation of internal losses. The implemented model was validated on many benchmarks from literature to compare the results with experimental and numerical results.

## 1 INTRODUCTION

During the modeling of hydraulic works, the engineer is lead to make many studies both on large scales and on smaller scales. The numerical studies on large scales cannot be carried out using 3D models because the high computational time would be many days. In another hand a classical 2D integrated approach on the water depth allows to achieve accurately this goal but only on a certain distance from the hydraulic structure. In the vicinity of the structure, the assumptions retained in the implementation of 2D integrated models, namely in particular the assumption on hydrostatic pressure are no more verified. In this vicinity, the flow develops vertical velocities which are not negligible anymore compared to the velocities developed in the horizontal plane.

In this case, the recourse to explicitly discretized models on the water height must be implemented to obtain accurate hydrodynamic results near the structure. 3D models can be maybe exploited, but the contribution of those compared to a 2D vertical

model lead to the conclusion that 2D vertical models can give enough responses with less computing time. Following this assessment, it is consequently judicious to turn to a reliable 2D hydrodynamic model allowing to describe accurately the local hydrodynamics.

Many interesting works are made up outfalls, local topographic steps and so on. However, this kind of singularities are often connected to a free surface flow, what is very difficult to manage numerically. The flows under pressure in tubes or closed channel have the advantages to propose a flow where the management of the free surface is not necessary. The program that is presented in this paper and that has been applied to many benchmarks deal with these incompressible flows.

The developed code belongs to the modeling unit WOLF, entirely developed at the University of Liege in unit HACH. This modeling system is made up of several programs solving the hydrological run off (WOLFHYDRO) [6], the flows in river networks (WOLF1D) [4], the two-dimensional flows by integrating on the water depth (WOLF2D) [3] and

finally the incompressible flows under pressure (WOLF2DV), what is presented in this paper.

All the developed softwares are based on the same architecture. The method of the finite volumes applied to structured grids is systematically used. The constant or linear reconstructions of variables are also systematically employed guaranteeing, spatially, the first or the second order of precision spatially. Moreover, temporal integrations are ensured by the popular schemes of Runge-Kutta going up to four steps.

This paper will include in section 1 the basic principles governing the dynamics of the flows in the vertical plane using the Navier-Stokes equations. A brief review of the methods used to solve these ones will be suggested. The method of projections which was adopted and developed initially by [2] will be detailed in its principles.

Section 2 will present the space and temporal discretizations that were carried out, as well as the implicit resolution of the Poisson's equation related to the method of projections.

Section 3 will propose several benchmarks based on numerical, theoretical and experimental results coming from the literature and showing the validity and accuracy of the implemented code.

## 2 FORMULATION OF THE NAVIER-STOKES EQUATION

In the vertical plane, the Navier-Stokes equations are composed by the conservation of the mass and the momentum balances that can be written in the general form [9]:

$$\begin{cases} \frac{\partial \rho}{\partial t} + \vec{\nabla} \cdot (\rho \vec{v}) = 0 \\ \frac{\partial \rho \vec{v}}{\partial t} + \vec{\nabla} \cdot (\rho \vec{v} \otimes \vec{v}) = -\vec{\nabla} p + \vec{\nabla} \cdot \vec{\tau} + \rho \vec{f} \end{cases} \quad (1)$$

Where  $\rho$  is the density,  $t$  the time,  $\vec{v}$  is the velocity field,  $p$  is the pressure,  $\vec{\tau}$  is the tensor of shear viscous stresses and  $\vec{f}$  is the field of external volume forces.

In the framework of the work detailed in this paper, some additional assumptions are put forward in order to simplify the Navier-Stokes equations:

- The density is supposed to remain constant in time and space and is noted  $\rho_0$ .
- Water is regarded as a newtonian fluid with the formalism of the tensor of shear viscous stresses that follows.
- The assumption of Stokes is kept in order to simplify the expression of the viscous constraints.

The use of these assumptions in the system of equations (1) leads to the following simplified expression:

$$\begin{cases} \vec{\nabla} \cdot \vec{v} = 0 \\ \frac{\partial \vec{v}}{\partial t} + \left( \vec{v} \cdot \vec{\nabla} \right) \vec{v} = -\frac{1}{\rho_0} \vec{\nabla} p + \text{div}(\nu \vec{\nabla} \vec{v}) + \vec{f} \end{cases} \quad (2)$$

Where  $\nu = \mu / \rho_0$  is the kinematic viscosity of the fluid and  $\mu$  is the dynamic viscosity or the shear stress viscosity of the fluid.

### 2.1 Conservative formulation

The formulation of the Navier-Stokes equations expressed in (2) represents the non conservative form of the advection terms. Essentially, this kind of formulation presents disadvantages during its numerical resolution by causing a global loss of the advected quantities. For this reason one generally prefers a conservative formulation which can be established by taking into account the null divergence property of the incompressible fluid. For example the first component of the advection term becomes:

$$\begin{aligned} & u \frac{\partial u}{\partial x} + v \frac{\partial u}{\partial y} \\ &= \frac{\partial u^2}{\partial x} + \frac{\partial uv}{\partial y} - u \underbrace{\left( \frac{\partial u}{\partial x} + \frac{\partial v}{\partial y} \right)}_{\vec{\nabla} \cdot \vec{v} = 0} \\ &= \frac{\partial u^2}{\partial x} + \frac{\partial uv}{\partial y} \end{aligned} \quad (3)$$

Where  $u$  and  $v$  are the velocities components in the horizontal and in vertical plane, respectively.

Finally, the integration of the only force of volume available (which is the gravity one) in the vertical gradient of pressure ensures to simplify the equation by moving the source term. Moreover the kinematic viscosity is kept constant in the case of laminar flows. The conservation of mass and the 2 equations of momentum balances to be solved are finally summarized as:

$$\begin{cases} \frac{\partial u}{\partial x} + \frac{\partial v}{\partial y} = 0 \\ \frac{\partial u}{\partial t} + \frac{\partial u^2}{\partial x} + \frac{\partial uv}{\partial y} + \frac{1}{\rho_0} \frac{\partial p^*}{\partial x} - \nu \left( \frac{\partial^2 u}{\partial x^2} + \frac{\partial^2 u}{\partial y^2} \right) = 0 \\ \frac{\partial v}{\partial t} + \frac{\partial v^2}{\partial y} + \frac{\partial uv}{\partial x} + \frac{1}{\rho_0} \frac{\partial p^*}{\partial y} - \nu \left( \frac{\partial^2 v}{\partial x^2} + \frac{\partial^2 v}{\partial y^2} \right) = 0 \end{cases} \quad (4)$$

Where  $p^*$  is a conventional pressure, the action of gravity being added to the hydrostatic pressure.

### 3 METHODS OF RESOLUTION

This chapter aims to present a rapid summary among the methods of resolution applied to the incompressible Navier-Stokes equations. For each of them, a short theoretical description is outlined and an enumeration of the principal advantages and disadvantages inherent to each method is sketched. The last described method, which is the projection's method, is the one which is adopted in the scope of this paper.

#### 3.1 Iterative implicit method

The process which is certainly the most intuitive one consists in transforming the system of equations in a quasi-linear form. After that one needs to solve this linear system described in [10]. As an illustration, the linearised system is presented below for an explicit temporal discretisation of Euler.

$$\begin{pmatrix} 0 & \vec{\nabla} \\ \frac{\Delta t \vec{\nabla}}{\rho_0} & I + \Delta t \vec{v} \cdot \nabla + \nu \nabla^2 \end{pmatrix} \begin{pmatrix} p^{n+1} \\ \vec{v}^{n+1} \end{pmatrix} = \begin{pmatrix} 0 \\ \vec{v}^n + \Delta t \vec{f}^{n+1} \end{pmatrix} \quad (5)$$

where  $I$  is the unit matrix. Many iterative methods exist for the resolution of such systems but they all have the disadvantages to consume huge computer resources such as the computational time or the needed memory. On the other hand, the principal advantage of these methods lies in the use of time steps larger than for the explicit methods.

#### 3.2 Artificial compressibility method

This process of resolution was introduced at the origin by [2] in 1967 and consists in introducing a pseudo temporal term in the equation of continuity. This modification transforms the initial system of elliptic equations into a hyperbolic one. The pseudo-pressure term disappears when the steady state is reached after several iterations on the complete system.

$$\begin{cases} \frac{1}{\beta^2} \frac{\partial p}{\partial t} + \vec{\nabla} \cdot \vec{v} = 0 \\ \frac{\partial \vec{v}}{\partial t} + \left( \vec{v} \cdot \vec{\nabla} \right) \vec{v} = -\frac{1}{\rho_0} \vec{\nabla} p + \nu \nabla^2 \vec{v} + \vec{f} \end{cases} \quad (6)$$

The term  $\beta$  contained in the equation of continuity has the dimensions of a velocity and represents actually a pseudo pressure wave celerity. In fact, the system corresponds to a compressible flow for very low MACH numbers. Of course, the transient behavior of the pressure loses, in the case of an incompressible fluid, all its physical signification and recovers its actual meaning when the pseudo-pressure term tends to zero.

A rather fast evaluation of the current number and the value of the parameter  $\beta$  [11; 8] allows to evaluate the order of magnitude of the time step that would be necessary to ensure the stability of the scheme:  $\Delta t \sim 10^{-5}$  seconds. This very low time step is the principal limitation of this method. In addition, the need to compute temporal pseudo iterations within a time step increases the computational time quite a lot.

#### 3.3 Projection method

This method is relatively simple to apprehend while providing a relatively powerful scheme of resolution. The multi-step approach scoped in this paper allows separating the initial equations to be solved together in an approach in two times. This process allows solving two types of equations met very often in fluid mechanics, for which numerical schemes were validated many times. Thus, the principle of resolution will be kept in order to solve the Navier-Stokes equation.

### 4 DETAILS ON THE PROJECTION METHOD

The projection of the equations in the vector space with null divergence allows to separate the resolution of the problem in two independent stages. The disappearance of the gradient pressure term prior to this phase makes possible to get from the momentum balances a purely convective equation, eventually with diffusive terms. These 2 equations are solved in order to provide an approximate velocity field usually noted  $\vec{V}^*$ . This is called the transport phase. This approximated field does not verify the constraint of null divergence specific to an incompressible flow, and it is consequently necessary to restore this last one.

To achieve this goal one can easily, by comparing the equations, link the approximate velocity field to the velocity field at the next time step as well as the gradient of the pressure field. In addition, the application of the divergence operator to these three fields ensures to eliminate the velocity field at the next time step and to find a relation between the Laplacian of the pressure and the divergence of the approximate velocity field. This equation is more commonly known as the Poisson's equation.

The resolution of this last one ensures to know the pressure field resulting from the incompressibility constraint in the flow, and in addition reflects its null divergence nature. This pressure field finally enables to modify the approximate velocity field  $\vec{V}^*$  into a null divergence field. This is known as the

projection step. At the end of these operations, the new values of the variables are known and can be used as a step predictor in a Runge-Kutta scheme or directly as the result at the next time step for a temporal integration of Euler.

#### 4.1 Solver's structure and numerical schemes

In this paragraph, we will describe the structure of resolution implemented in the solver, as well as the schemes and numerical methods used for the resolution of the equations. As explained before, the modeling system developed in the HACH is exclusively based on the principle of the finite volumes, applied to structured grids. Temporal integrations are ensured by Runge-Kutta schemes, which can be seen as a result of several Euler steps, as shown on Figure 1.

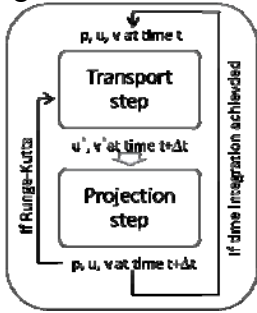


Figure 1: Sketch of the resolution scheme for the projection method

##### 4.1.1 Discretisation of the transport step

In the purpose of clearness, the developments established hereafter will be limited to an explicit temporal discretisation of Euler in order to describe the different stages of the resolution. It is clearly understood that more advanced temporal schemes can be implemented in order to confer on the modellings a temporal evolution of an adequate precision.

Based on a semi-implicit temporal discretisation on pressure, from step  $n$  (at time  $t$ ) to step  $n+1$  (at time  $t+\Delta t$ ), the equations can be written as :

$$\begin{cases} \frac{\partial u^{n+1}}{\partial x} + \frac{\partial v^{n+1}}{\partial y} = 0 \\ \frac{u^{n+1} - u^n}{\Delta t} + \frac{\partial u^n}{\partial x} + \frac{\partial v^n}{\partial y} + \frac{1}{\rho_0} \frac{\partial p^{*n+1}}{\partial x} - \nu \left( \frac{\partial^2 u^n}{\partial x^2} + \frac{\partial^2 u^n}{\partial y^2} \right) = 0 \\ \frac{v^{n+1} - v^n}{\Delta t} + \frac{\partial v^n}{\partial y} + \frac{\partial u^n}{\partial x} + \frac{1}{\rho_0} \frac{\partial p^{*n+1}}{\partial y} - \nu \left( \frac{\partial^2 v^n}{\partial x^2} + \frac{\partial^2 v^n}{\partial y^2} \right) = 0 \end{cases} \quad (7)$$

According to the Hodge's theorem that enables to eliminate the pressure term, the 2 equations of momentum balance can be solved to determine the approximate velocity field  $(u^*, v^*)$ . This velocity field does not check, at this moment, the condition of null divergence. Consequently the incompressible character of the fluid is not yet restored.

$$\begin{cases} u^* = u^n - \Delta t \left( \frac{\partial u^n u^n}{\partial x} + \frac{\partial u^n v^n}{\partial y} - \nu \left( \frac{\partial^2 u^n}{\partial x^2} + \frac{\partial^2 u^n}{\partial y^2} \right) \right) \\ v^* = v^n - \Delta t \left( \frac{\partial v^n v^n}{\partial y} + \frac{\partial u^n v^n}{\partial x} - \nu \left( \frac{\partial^2 v^n}{\partial x^2} + \frac{\partial^2 v^n}{\partial y^2} \right) \right) \end{cases} \quad (8)$$

The reconstruction of the variables at the edges of each finite volume can be constant and thus ensuring a 1<sup>st</sup> order of precision, or linear one by using the values in the center of closest finite volumes (2<sup>nd</sup> order of precision). The use of the diffusive terms is optional. However, taking into account these ones immediately implies to use the second order of precision spatially, in order to limit the numerical diffusion of the advective terms.

##### 4.1.2 Discretisation of the projection step

In order to build a null divergence velocity field, an identification between (7) and (8) enables to find a link between the approximate velocity field and the gradient of pressure:

$$\begin{cases} u^* = u^{n+1} + \Delta t \frac{1}{\rho_0} \frac{\partial p^{*n+1}}{\partial x} \\ v^* = v^{n+1} + \Delta t \frac{1}{\rho_0} \frac{\partial p^{*n+1}}{\partial y} \end{cases} \quad (9)$$

These last equations still contain the two velocity unknowns at next time step. This is why the divergence operator is applied to the approximate velocity field. Using the first equation of (7), one can easily find the following relation between the pressure and the approximate velocity field.

$$\frac{\partial^2 p^*}{\partial x^2} + \frac{\partial^2 p^*}{\partial y^2} = \frac{\rho_0}{\Delta t} \left( \frac{\partial u^*}{\partial x} + \frac{\partial v^*}{\partial y} \right) \quad (10)$$

The resulting equation is in fact a Poisson's equation in which the source term is represented by the divergence of the approximate velocity field.

In the scheme implemented in the solver, this divergence is calculated by using on each edge of the finite volume the average value of each node close to the edge.

##### 4.1.2.1 Boundary conditions

If some velocity boundary conditions on the entrance or on the exit are imposed in the problem, they are directly imposed on the concerned edge when computing the transport phase. Thus, for a prescribed velocity, we have on the edges affected:  $u=u^*$  and  $v=v^*$ .

Boundary conditions of pressure, if they exist in the problem, are prescribed on the center of a fictitious cell located outside the computed domain as shown on Figure 2. This choice results from the central scheme used in the Poisson's equation. So, in order to impose a pressure  $P$  on the edge, one needs to impose  $P+dp$  on the closest node.

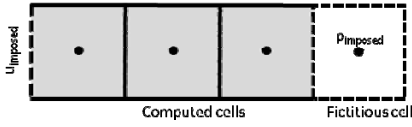


Figure 2 : Prescription of boundary conditions

#### 4.1.3 Resolution of the Poisson's equation

The Poisson's equation (10) is solved on the basis of a centered discretization of the unknown of pressure. In the purpose of solving problems presenting a significant number of unknowns which will constitute the modelings carried out, the explicit techniques of resolution of linear systems are avoided. In this paper, one directly prefers to them the improved implicit iterative method of the GMRES. In order to optimize the resolution of the linear system by the GMRES, one needs to make some preprocessing to limit the band width of the unknowns matrix, and to construct a good preconditioned matrix.

The band width of the unknowns matrix is of primary importance since this one influences basically the computing time. To achieve this goal, a classification of the unknowns according to the principle of an oil spot is programmed. This one ensures to limit the band width of the coefficient matrix to the maximum.

In addition, the width of the preconditioned matrix can be parameterized. The more important the width is, the less the number of iterations needed to reach the solution with the GMRES is. In another hand, an important memory capacity must be used and the computing time must be affected for the calculation of this preconditioned matrix. Thus there is an optimum between the calculation cost per iteration on the preconditioned matrix and the filling of this matrix.

Figure 3 illustrates the computing time for 2 different bandwidths and for different preconditioning of the coefficient matrix in the case of a rectangular zone filled by 32.000 cells.

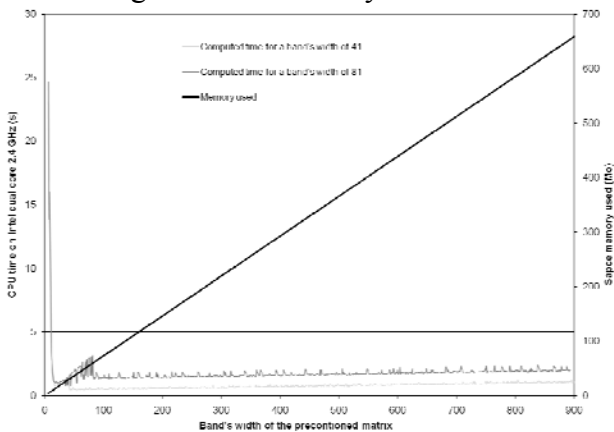


Figure 3 : GMRES computing time for different preconditioning parameters

#### 4.1.3.1 Restoring the null divergence

The resolution of the Poisson's equation ensures to restore the incompressibility nature of the fluid and to determine the field of pressure. In addition, the gradients of pressure which are calculated at the edges of the finite volumes enable to correct the approximate velocity field following the equation:

$$\begin{cases} u^{n+1} = u^* - \Delta t \frac{1}{\rho_0} \frac{\partial p^{*n+1}}{\partial x} \\ v^{n+1} = v^* - \Delta t \frac{1}{\rho_0} \frac{\partial p^{*n+1}}{\partial y} \end{cases} \quad (11)$$

Finally, the velocity field and the actual field of pressure are obtained. If Runge-Kutta iterations are calculated, it is suitable to start again the whole procedure described above, and to finally combine the solutions obtained according to the coefficients of the temporal scheme chosen.

## 5 APPLICATIONS

### 5.1 Flow over a backward facing step

#### 5.1.1 Numerical comparison

As a first application of the method, this section considers the two-dimensional channel flow over a backward facing step. This is a standard problem for which it exists several sources of numerical results to compare with. In particular, we shall compare our numerical results with those of Gartling [5] for a Reynolds number based on the flow rate equal to 800. The resolution method developed by Gartling is a Galerkin-based finite element method. This method is strictly different from the one developed in this paper but it allows to reach the same precision on the results.

The geometry of the flow in a non-dimensional coordinate system with channel dimensions, and the BCs used, are given in Figure 4. The characteristic length of the channel is the height  $H$ . For  $x \geq 0$ , the channel dimensions ( $0 \leq x \leq 30, -1/2 \leq y \leq 1/2$ ) are the same as [5]. The pressure imposed at the outlet of the channel is 0. At the inlet, a horizontal parabolic velocity is imposed according to the law  $u(y) = 24y(0.5 - y)$  and a null vertical velocity is considered in ( $x=0, 0 \leq y \leq 1/2$ ). The maximum velocity is consequently 1.5 m/s, while the average value is 1 m/s. A no slip condition is imposed on the walls.



Figure 4 : Backward facing step geometry with channel dimensions and BCs.

To check the numerical results, we have simulated the same Reynolds number considered in [5]. This

Reynolds number is  $Re=800$ . Considering the average velocity value of 1 m/s and a channel's height of 1m, the kinematic viscosity allowing to obtain the Reynolds number defined by Gartling is  $\nu=125 \cdot 10^{-6} \text{ m}^2/\text{s}$ .

Modellings are carried out on the basis of a mesh size of 2.5 cm (48 000 squared cells computed) by considering a linear reconstruction of the variables in order to limit the numerical diffusion of the advective terms.

It should be specified that the results of the pressure field proposed by Gartling are adjusted in a way to obtain a null pressure in (0,0). The same adjustment is done here. Since this point is singular, we do not have exactly the same shift as Gartling and this explains the small constant shift that one can see on some curves. The results obtained are illustrated on Figure 5 which represents the stabilized pressure field and the isovalues every 1 cm.

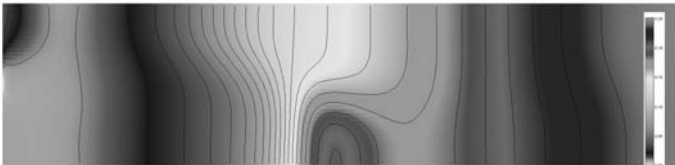


Figure 5 : Field of pressure (vertical stretch of 3) and isopressure lines.

Figure 6 shows some comparisons of the pressure field along two cuts in the channel. The cuts are made in  $x=7\text{m}$  and  $x=15\text{m}$ .

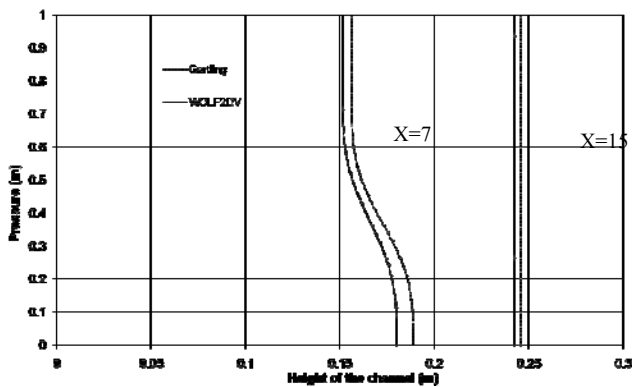


Figure 6 : Pressure profiles across the channel at  $x=7$  and  $x=15$ . A comparison can also be carried out along longitudinal cuts. Figure 7 shows that the modelled curves are practically superimposed on the curves digitalized from the paper version of Gartling.

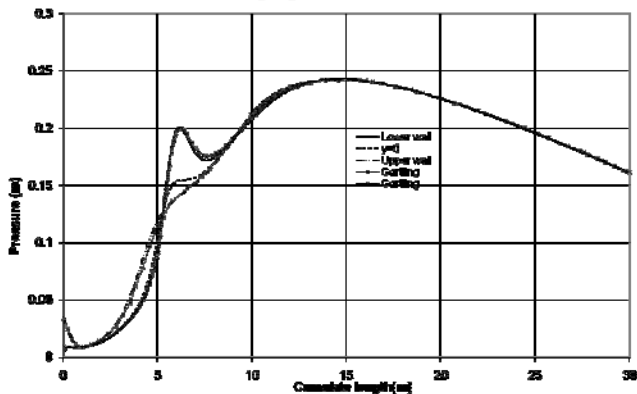


Figure 7 : Pressure profiles along the channel.

A comparison with the horizontal and vertical velocities is showed on Figure 8 and Figure 9. These ones are practically superimposed on the curves provided by Gartling and prove the validity of the implemented solver. A small deviation is observed on Figure 9 but it must be put in the context of very low vertical velocities present in the entirety of the computed domain.

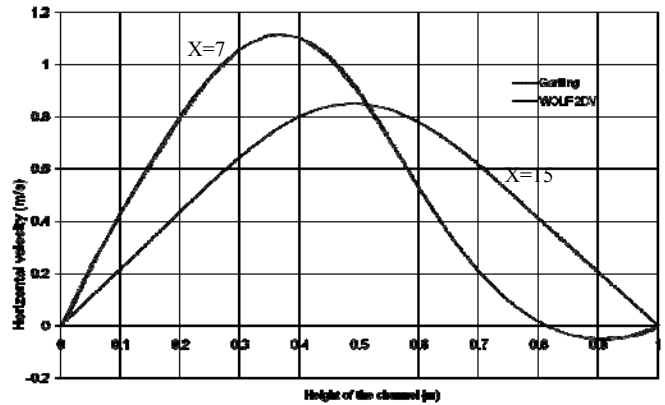


Figure 8 : Horizontal velocity profiles across the channel at  $x=7$  and  $x=15$ .

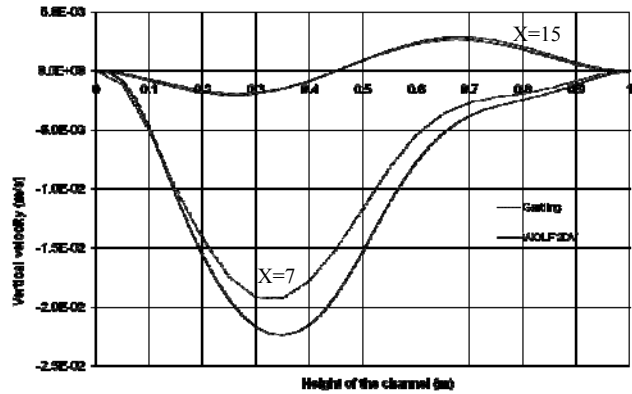


Figure 9 : Vertical velocity profiles across the channel at  $x=7$  and  $x=15$ .

### 5.1.2 Experimental comparison

A comparison with experimental results of [1] and numerical results of [1], [7] can also be carried out. This one has been carried out thanks to a lot of experiments in a channel with the same configuration as the one presented on Figure 4. The experiments provide results of the length of an adimensional recirculation ( $X/H$ ). This recirculation characterises the lower principal swirl observed in the channel.

$X$  represents the length of the recirculation and  $H$  the height of the channel. The shape and the length of this swirl vary according to the Reynolds number observed. In order to take into account the variation of this number, kinematic viscosity is calculated by keeping the mean velocity and the characteristic height constant. Figure 10 shows a very good agreement of the experimental length and the numerical recirculation for Reynolds number down to 500. For higher Reynolds numbers, a discordance appears. This one occurs according to the

appearance of three-dimensional turbulent structures [7], which are not taken into account in the model presented here.

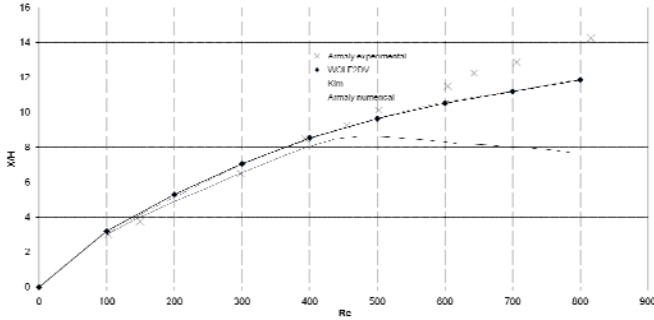


Figure 10 : Length of recirculation by Armaly, Kim and WOLF2DV.

## 5.2 Laminar flow over a flat plate

This example, known as Blasius flow, models boundary layer along a flat plate. This case is very famous because it proposes an analytical solution for the flow ensuring to adequately validate a solver of the Navier-Stokes equations [9]. The simulated domain is represented on Figure 11. The plate has a length of  $L=2$  m and begins in  $x=0$ . The inlet boundary condition is a uniform velocity ( $U=1$ ) and is placed at  $x=-0.67$  in order to capture the flow on the leading edge of the plate. The outlet boundary condition is placed at  $x=2$  and is a null pressure. The solution of Blasius is based on the assumption of a semi infinite extent upwards. This is obviously not possible in the framework of a numerical modeling. To remedy the problem, a boundary condition of pressure that ensures the fluid to get away is prescribed. This boundary condition is placed at  $y=0.62$  so that the flow remains homogeneous from this ordinate.

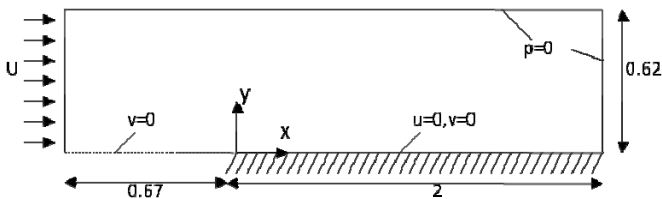


Figure 11 : Laminar flow over a flat plate: geometry and boundary conditions.

The analytical solution for the friction coefficient is :

$$C_f = \frac{0.664}{\sqrt{Re_x}} \text{ with } Re_x = \frac{U_\infty x}{\nu} \quad (12)$$

Where  $U_\infty$  is the far velocity in  $y=0.62$ .

The theoretical horizontal and vertical velocities are:

$$\frac{u}{U_\infty} = f'(\eta) \quad (13)$$

and

$$\frac{v}{U_\infty} \sqrt{Re_x} = \frac{1}{2} (\eta f'(\eta) - f(\eta)) \quad (14)$$

where  $\eta$  is the adimensional coordinate equals to  $\frac{y}{x} \sqrt{Re_x}$  and  $f$  is the solution of the Blasius equation.

The problem is equivalent to the one that consists in modelling a fluid at rest with a plate moving at the velocity  $U$ . The boundary layer which is developed in this flow is proportional to  $\sqrt{1/Re_x}$  and thus a very fine grid is necessary when one wants to model this layer explicitly. In another hand, the singularity in the pressure at the leading edge of the plate is another source of difficulty. By choosing a kinematic viscosity of  $\nu=0.001$  m<sup>2</sup>/s, the Reynolds number of the flow is:

$$Re_L = \frac{UL}{\nu} = 2000 \quad (15)$$

Consequently, the boundary layer is about 2 cm thick on the leading edge of the plate. The case modelled in this article uses squared cells with a constant size of 5 mm which allows to discretize the boundary layer for the kinematic viscosity chosen. The computed domain counts approximately 66.000 cells. Again, taking into account the diffusive terms forces to use the linear reconstruction.

The validation of the results is presented for a stabilized modeling. Figure 12 and Figure 13 compare the evolution of the friction coefficient computed along the plate with the solution suggested by Blasius (12).

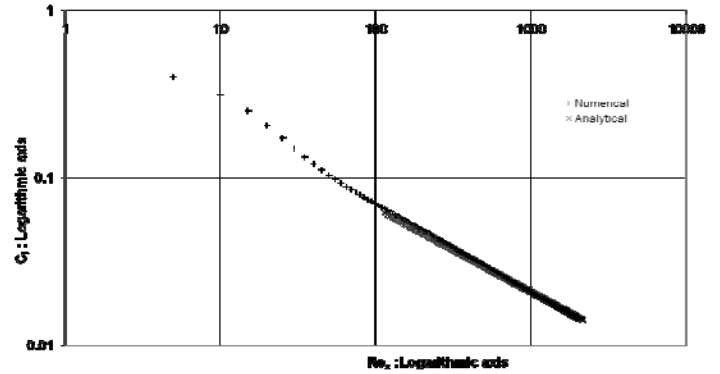


Figure 12: Laminar flow past a flat plate: skin friction distribution, both axis are logarithmic.

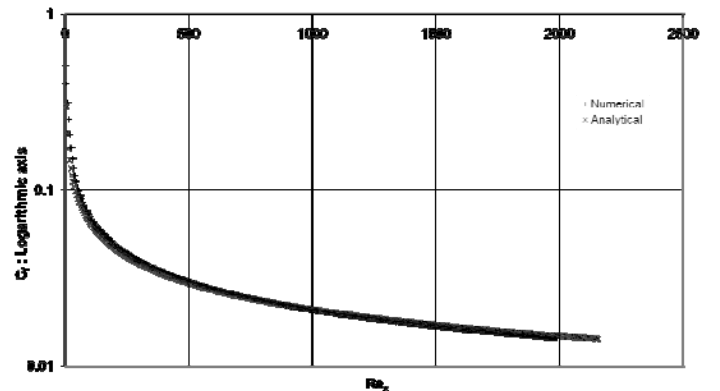


Figure 13 : Laminar flow past a flat plate: skin friction distribution, one axis is logarithmic.

Velocities computed in  $x=0.5$ ,  $x=1$  and  $x=1.5$  are compared to the analytical solutions of (13) and (14) on Figure 14 and Figure 15.

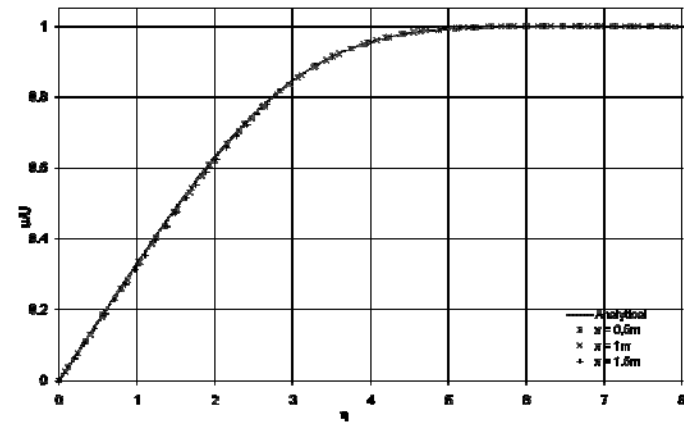


Figure 14: Longitudinal velocity.

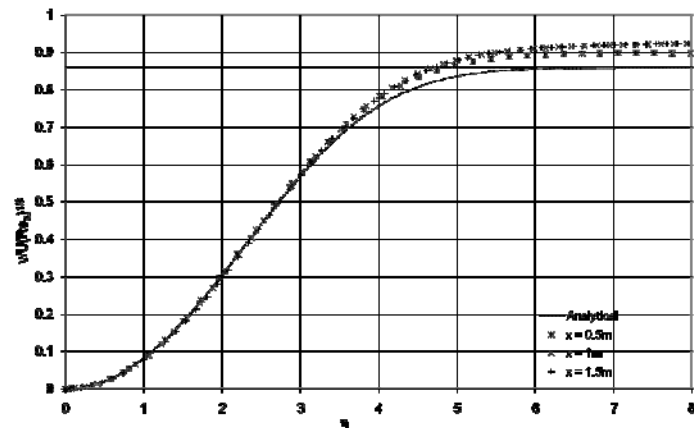


Figure 15: Vertical velocity.

## 6 CONCLUSIONS

This paper presents a finite volumes method enabling to solve the incompressible Navier-Stokes equations in the vertical plane of the flow. The boundary conditions can be imposed as velocities but also as pressure fields. The explicit numerical schemes suggested ensure to reach a temporal or spatial precision of the second order. By elsewhere, the scheme of resolution proposed makes it possible to solve systems made up of several hundred thousands of unknowns, thanks to the implicit resolution of the Poisson's equation. In particular, the scheme of second order in time and space ensured to evaluate the qualities of the solver on 2 benchmarks based on numerical, experimental and analytical methods. The comparison was very good for each case.

This promising method must now be extended to cases where a free surface is present and must be treated in an explicit way during the entire calculation.

## 7 NOTATIONS

$\rho, \rho_0 =$  water density

$x =$  coordinate along horizontal axis

$y =$  coordinate along vertical axis

$t =$  time

$g =$  gravity acceleration

$\vec{v} =$  velocity field

$p, p^* =$  pressure

$\vec{\tau} =$  tensor of shear viscous stresses

$\vec{f} =$  field of external volume forces

$\nu =$  kinematic viscosity

$\mu =$  dynamic viscosity

$u, u^* =$  horizontal component of the velocity field

$v, v^* =$  vertical component of the velocity field

$\Delta t =$  time step

$C_f =$  friction coefficient

$Re =$  reynolds number

$\eta =$  non-dimensional coordinate of Blasius

$f(\eta) =$  solution of Blasius equation

## 8 REFERENCES

- [1] Armaly, F., F. Durst, J. C. F. Pereira et B. Schonung, Experimental and Theoretical Investigation of Backward Facing Step Flow. *Journal of Fluid Mechanics*, 1983. 127: p. 473-496.
- [2] Chorin, A. J., Numerical method for solving incompressible viscous flow problem. *Journal of computational physics*, 1967. 2: p. 12-20.
- [3] Erpicum, S., P. Archambeau, S. Detrembleur, B. J. Dewals et M. Piroton, Detailed flood extension forecasting in the Walloon region with a 2D finite volume multiblock free surface flow solver. *4th Int. Conf. on Advanced Computational Methods in Engineering*, Liege, Belgium, 2008.
- [4] Erpicum, S., P. Archambeau, B. Dewals, S. Detrembleur & M. Piroton, Optimisation of hydroelectric power stations operations with WOLF package. *5th International Conference on Hydropower*, Stavanger, 2005.
- [5] Gartling, D. K., A test problem for outflow boundary conditions - Flow over a backward-facing step. *International journal for numerical method in fluids*, 1990. 11: p. 953-967.
- [6] Khuat Duy, B., P. Archambeau, B. J. Dewals, S. Erpicum et M. Piroton, Modelling of sewer systems as a component of a global hydrological model. *4th Int. Conf. on Advanced Computational Methods in Engineering*, Liege, Belgium, 2008.
- [7] Kim, J., Moin, P., Application of a fractional-step method to incompressible Navier-Stokes equations. *Journal of computational physics*, 1985. 59: p. 308-323.
- [8] Mouzelard, T. Contribution à la modélisation des écoulements quasi-tridimensionnels instationnaires à surface libre. *Université de Liège, Faculté des Sciences Appliquées, département ArGEnCo*, 2002.
- [9] Schlichting, H. Boundary layer theory. *McGraw-Hill*, New York, 1968.
- [10] Studer, L. Modelling the vertical centrifugal casting of large bimetallic rolling mills. *Université de Liège*, 2007.
- [11] Versteegh, J. Numerical simulation of three-dimensional flow through or around hydraulic structures. *Delft Technological University*, 1990.